



HAL
open science

Imaging the lithospheric structure beneath the Indian continent

S. Maurya, J. -P. Montagner, M. Ravi Kumar, E. Stutzmann, S. Kiselev, G. Burgos, N. Purnachandra Rao, D. Srinagesh

► **To cite this version:**

S. Maurya, J. -P. Montagner, M. Ravi Kumar, E. Stutzmann, S. Kiselev, et al.. Imaging the lithospheric structure beneath the Indian continent. *Journal of Geophysical Research: Solid Earth*, 2016, 121, pp.7450-7468. 10.1002/2016JB012948 . insu-03581279

HAL Id: insu-03581279

<https://insu.hal.science/insu-03581279>

Submitted on 19 Feb 2022

HAL is a multi-disciplinary open access archive for the deposit and dissemination of scientific research documents, whether they are published or not. The documents may come from teaching and research institutions in France or abroad, or from public or private research centers.

L'archive ouverte pluridisciplinaire **HAL**, est destinée au dépôt et à la diffusion de documents scientifiques de niveau recherche, publiés ou non, émanant des établissements d'enseignement et de recherche français ou étrangers, des laboratoires publics ou privés.

Copyright

RESEARCH ARTICLE

10.1002/2016JB012948

Key Points:

- New massive surface wave data set assembled for this work
- First high-resolution 3-D shear wave velocity model for the Indian continent
- Our 3-D model explains most of the geological features and different cratonic blocks

Supporting Information:

- Supporting Information S1
- Table S1

Correspondence to:

S. Maurya,
maurya@ipgp.fr

Citation:

Maurya, S., J.-P. Montagner, M. R. Kumar, E. Stutzmann, S. Kiselev, G. Burgos, N. P. Rao, and D. Srinagesh (2016), Imaging the lithospheric structure beneath the Indian continent, *J. Geophys. Res. Solid Earth*, 121, 7450–7468, doi:10.1002/2016JB012948.

Received 23 FEB 2016

Accepted 6 OCT 2016

Accepted article online 8 OCT 2016

Published online 30 OCT 2016

Imaging the lithospheric structure beneath the Indian continent

S. Maurya¹, J.-P. Montagner¹, M. Ravi Kumar², E. Stutzmann¹, S. Kiselev³, G. Burgos¹, N. Purnachandra Rao², and D. Srinagesh²

¹Institut de Physique du Globe de Paris, Paris, France, ²National Geophysical Research Institute, Hyderabad, India, ³Institute of Physics of the Earth, Moscow, Russia

Abstract We present a high-resolution 3-D lithospheric model of the Indian plate region down to 300 km depth, obtained by inverting a new massive database of surface wave observations, using classical tomographic methods. Data are collected from more than 550 seismic broadband stations spanning the Indian subcontinent and surrounding regions. The Rayleigh wave dispersion measurements along ~14,000 paths are made in a broad frequency range (16–250 s). Our regionalized surface wave (group and phase) dispersion data are inverted at depth in two steps: first an isotropic inversion and next an anisotropic inversion of the phase velocity including the *SV* wave velocity and azimuthal anisotropy, based on the perturbation theory. We are able to recover most of the known geological structures in the region, such as the slow velocities associated with the thick crust in the Himalaya and Tibetan plateau and the fast velocities associated with the Indian Precambrian shield. Our estimates of the depth to the Lithosphere-Asthenosphere boundary (LAB) derived from seismic velocity V_{sv} , reductions at depth reveal large variations (120–250 km) beneath the different cratonic blocks. The lithospheric thickness is ~120 km in the eastern Dharwar, ~160 km in the western Dharwar, ~140–200 km in Bastar, and ~160–200 km in the Singhbhum Craton. The thickest (200–250 km) cratonic roots are present beneath central India. A low velocity layer associated with the midlithospheric discontinuity is present when the root of the lithosphere is deep.

1. Introduction

The Indian plate, since breakup from the Gondwanaland ~130 Ma ago, is quite unique compared to the other major Gondwana fragments—Australia, Africa, Antarctica, and South American plates. During the Cretaceous-Tertiary period, the Indian lithosphere separated from Antarctica-Australia at ~130 Ma, from Madagascar at ~90 Ma, and from Seychelles at ~65 Ma. Subsequently, it was ravaged by four major plumes, namely, the Reunion, Marion, Kerguelen, and Crozet. In particular, interaction between the Reunion plume and the Indian lithosphere led to a major volcanic event around 65 Ma ago. The eruptions occupy more than 500,000 km² on the western and central portions of the Indian shield called the Deccan Volcanic Province (DVP). Also, the Indian plate moved northward at very high velocities of ~18–20 cm/yr during the Cretaceous [McKenzie and Sclater, 1971; Patriat and Achache, 1984; Klootwijk et al., 1992] and slowed down to 4–5 cm/yr after continental collision with Asia at ~50 Ma. The collision created the world's highest mountain chain, the Himalaya, and the tallest plateau, the Tibetan plateau.

The Indian subcontinent is a mosaic of various Precambrian cratons (Figure 1). The cratonization was a multi-phase process which completed and stabilized around 2.5 Ga [Meert et al., 2010]. These cratons are separated by different geological features [Raval and Veeraswamy, 2003b] such as mobile belts and rifts. The prominent ones are the Delhi-Aravalli, Satpura, and the Eastern Ghat mobile belts and the Godavari, Mahanadi, Narmada-Son, Cambay, and Kutch rifts. However, in regions blanketed by the Deccan volcanic traps or sediments (e.g., beneath DVP: CB-DVP and Bundelkhand), the craton boundaries are not so well defined on the surface. The central portion of the Indian shield is mostly covered by thick (up to ~8 km) quaternary sediments originating from the Himalaya. Thick sediments are also prevalent in the Himalaya, the Indo-Gangetic plain (IGP), and the Bay of Bengal where the basement depth is between 6 and 16 km.

Previous studies of the lithospheric structure based on heat flow data beneath the Indian continent [Negi et al., 1986] suggest the existence of a thin lithosphere beneath the old cratonic nuclei. This was attributed as the cause for the fast drift and supermobility of the Indian plate. The Lithosphere-Asthenosphere boundary (LAB) beneath diverse tectonic settings in India inferred using receiver functions [Kumar et al., 2007, 2013]

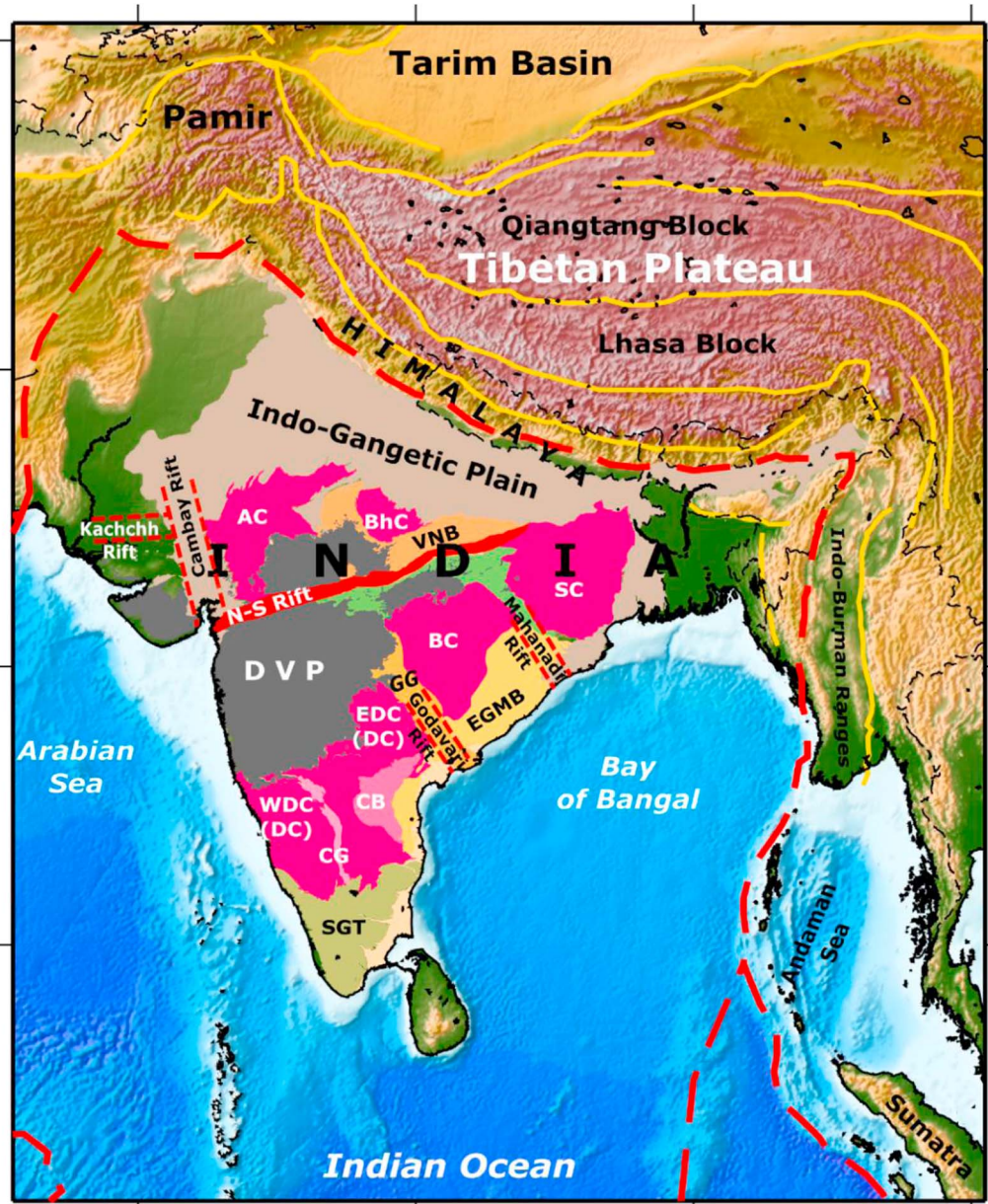


Figure 1. Simplified geological setting showing major tectonic features of India and surrounding regions (modified after GSI and ISRO [1994]). The cratons are: Easter Dharwar (EDC, 2700 Ma), Western Dharwar (WDC, 3600 Ma), Bastar (BC, 3500 Ma), Singhbhum (SC, 3500-3800 Ma), Aravalli (AC, 3500 Ma), and Bundelkhand (BhC, 3300 Ma). Age of the cratons is taken from Meert *et al.* [2010]. Red dashed lines are the plate boundaries [DeMets *et al.*, 1990].

also suggests absence of deep high-velocity lithospheric roots. This is counter intuitive to the scenario commonly expected beneath cratonic regions. However, these observations of a thin lithosphere cannot be easily reconciled with the thick lithospheric roots (high-velocity anomalies) revealed by the recent body wave [Singh *et al.*, 2014] and surface wave studies [Mitra *et al.*, 2006a]. Also, thermobarometric analysis of xenoliths derived from kimberlite samples suggests a thick lithosphere beneath the Dharwar Craton (~230 km at ~1.0 Gyr) and the Bastar Craton (~175 km at ~65 Myr) [Babu *et al.*, 2009]. Similar results were also found from joint interpretation of magnetotelluric and seismic tomography models [Naganjaneyulu and Santosh, 2012], as well as heat flow and temperature profiles derived from xenolith data beneath the Eastern Dharwar Craton.

Clearly, there appears to be discrepancies in the lithospheric thickness derived from different approaches like seismic tomography, receiver functions, magnetotellurics, heat flow, and xenolith studies, which is a matter of debate. A similar discrepancy in North America [Rychert and Shearer, 2009] was explained by the existence of a midlithospheric discontinuity (MLD) [Yuan and Romanowicz, 2010]. At present, it is widely agreed [Fouch and Rondenay, 2006; Abt *et al.*, 2010; Selway *et al.*, 2015] that a velocity drop occurs at the MLD.

Several surface wave studies [Bhattacharya, 1974, 1981; Mitra *et al.*, 2006a, 2006b; Acton *et al.*, 2010] were carried out for the Indian plate, but none of these studies yielded a complete picture of the 3-D structure. In the present work, we investigate the lithospheric structure and attempt to map the LAB and the MLD of the Indian plate using surface waves recorded at a dense network of seismic stations. Our main focus is on deciphering the lateral variation of the lithospheric structure and thickness beneath different cratonic blocks through a detailed 3-D modeling of the Indian plate. We follow the technique of classical surface wave tomography to derive a high-resolution 3-D tomographic model including anisotropy of the lithosphere of the Indian plate. We utilize vast amount of data collected from more than 550 seismic broadband stations in order to obtain a good spatial and azimuthal coverage. We measure ~14,000 group and phase velocities for the fundamental mode of the surface waves sampling the Indian plate. This dispersion data set is incorporated in a two-step (plus an intermediate step) inversion procedure to obtain the 3-D anisotropic model.

2. Data Selection and Processing

For the first time, we assembled a massive surface wave data set spanning the Indian subcontinent and surrounding regions, to image the shear velocity structure with high resolution. Three component waveforms are extracted from 29 global and regional broadband seismic networks comprising over 550 seismic stations (Figure 2). The seismic waveforms from the global stations are retrieved from the Incorporated Research Institutions for Seismology-Data Management Center (IRIS-DMC) and one additional network (YV-2011) of the RHUM-RUM project, using the ObspyDMT package [Scheingraber, 2013]. The data from the regional networks are acquired from various stations operated by the Indian organizations, like the National Geophysical Research Institute (NGRI), the Indian Meteorological Department (IMD) in different areas of the Indian shield, and the Indian Institute of Technology Bombay (IITB) network located in the Deccan volcanic province and northwest India. Based on the global centroid moment tensor database [Dziewonski *et al.*, 1981], we select waveforms of earthquakes of magnitude $M_w > 5.5$ (Figure 2c). The preprocessing steps such as removing the instrument response, mean, trend, tapering, filtering, and filling headers with source and receiver information are performed using the Seismic Analysis Code (SAC). We manually picked good quality seismograms with a focus on the amplitude of the fundamental mode, which should be well above the background noise. The Rayleigh wave data comprise a good azimuthal coverage (Figure 3) especially for the Indian shield, Tibet, Himalaya, and the Bay of Bengal.

3. Measurements of Surface Wave Dispersion

Investigation of the lithospheric structure using surface waves requires a high-resolution model of shallow layers because surface waves are strongly sensitive to the shallow structure [Montagner and Tanimoto, 1991; Boschi and Ekström, 2002; Marone and Romanowicz, 2007; Ferreira *et al.*, 2010]. We measure the dispersion curves of the fundamental mode of surface waves in a broad period range of 16–250 s. The dispersion data set is prepared for group velocity in the period range of 16–200 s and phase velocity in the range of 36–250 s. The group velocity measurements are extended down to short periods (16 s) in order to obtain

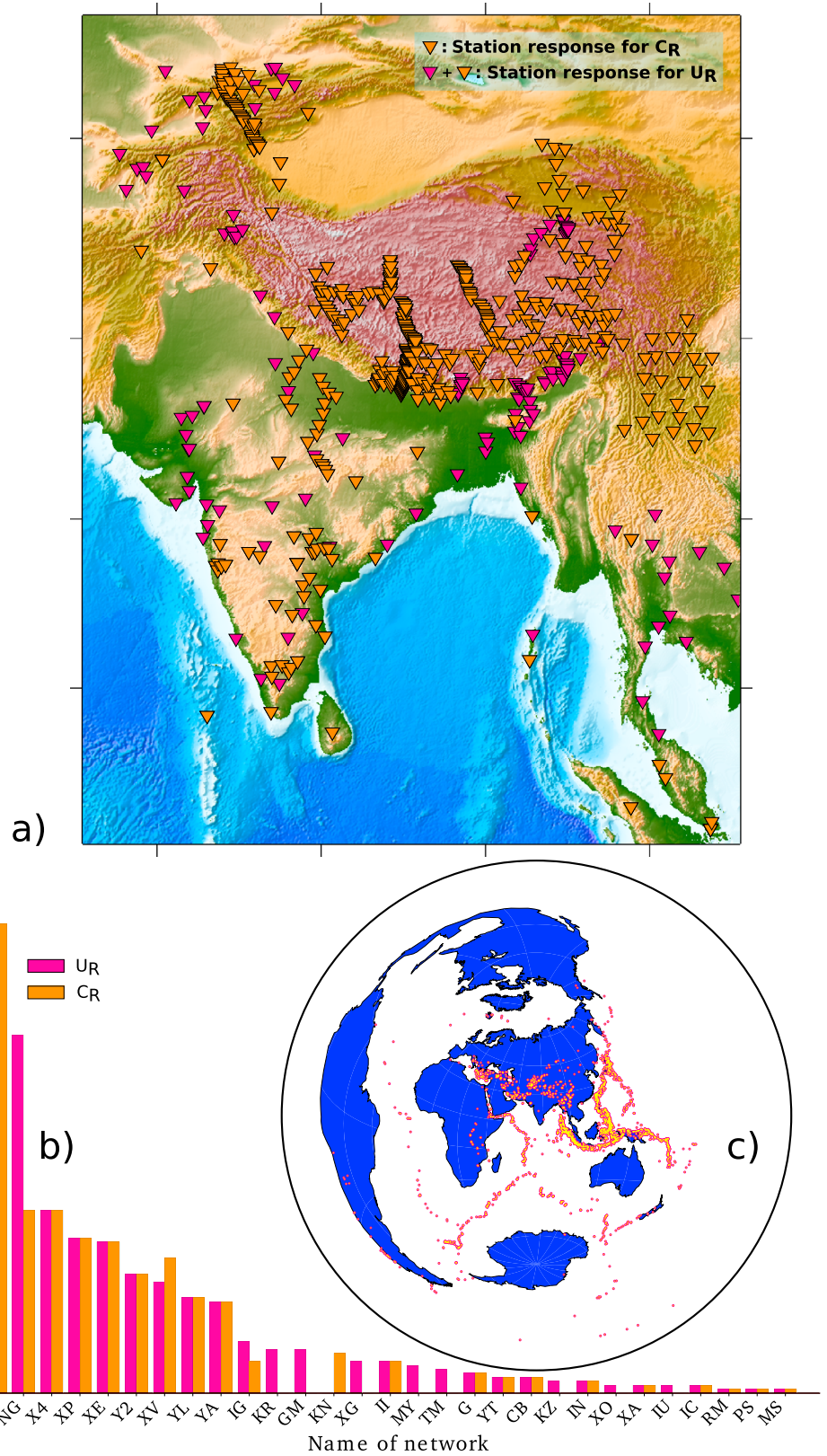


Figure 2. (a) Geographical distribution of the seismic broadband stations (inverted triangles) (see SI Figure S1 for information about the rest of stations sited outside the study region). (b) Bar diagram showing the number of stations in each network that yielded usable group (U_R) and phase (C_R) velocity measurements. (c) Epicenters of the earthquakes.

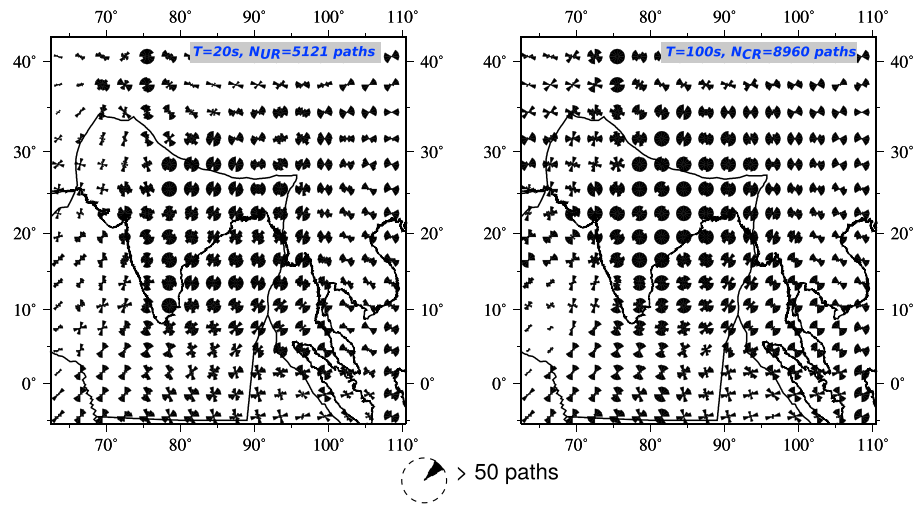


Figure 3. Azimuthal coverage of the (left) Rayleigh wave group and (right) phase data at 20 and 100 s with the respective number of paths N_{UR} and N_{CR} (in top right). The number of paths per unit area ($3^\circ \times 3^\circ$ cell) is binned in an azimuth range of 30° and the vectors are saturated at 50 paths. We present similar plots for other periods in SI Figures S1.2 and S1.3.

better constraints on the crust. The Rayleigh wave dispersion database consists of group velocity (U_R) along ~8000 paths and phase velocity (C_R) measurements along ~6000 paths.

3.1. Group Velocity Measurements

The average group velocity of Rayleigh waves between the sources and receivers in the period range of 16–250 s is measured using the frequency-time analysis method [Levshin *et al.*, 1989] (code automated by Mordret *et al.* [2015]). However, for some events, the automatic picking of the dispersion curves is complex, especially at short periods, due to scattered waves, multipathing, and overtones. To remove bad measurements, we considered individual dispersion curves and visually picked only that portion of the frequency band where the group dispersion curve is well defined and clear. An example of the group velocity dispersion curve is shown in supporting information Figure S2.1.

3.2. Phase Velocity Measurements

The largest wave train is usually associated with the fundamental mode of Rayleigh and Love waves but to avoid contamination due to overtones we use the Roller coaster algorithm [Beucler *et al.*, 2003] to retrieve the average phase velocity of the fundamental mode ($n=0$) along each path. A complete exploitation of the overtone data will be presented in another paper.

The seismogram $A_R e^{i\phi^R}$ recorded at a receiver “R” due to a source “S” can be expressed in the Fourier domain as

$$A^R(r, \omega) \exp[i\phi^R(r, \omega)] = \sum_{j=0}^n A_j^S(r, \omega) \exp\left\{i\left[\phi_j^S(r, \omega) + \frac{\omega a \Delta}{C_j^S(r, \omega)} p_j(r, \omega)\right]\right\}, \quad (1)$$

where $p_j(r, \omega) = \frac{C_j^R(r, \omega) - C_j^S(r, \omega)}{C_j^S(r, \omega)}$, “a” is the radius of Earth, Δ is the epicentral distance in radians, $\phi^S(\omega)$ is the source phase, C_j^R is the phase velocity of the j th mode averaged along the great-circle path, and C_j^S is the synthetic phase velocity computed from the 1-D reference Earth model. The steps involved in the “roller coaster” method are discussed in the SI Figure S2.

3.3. Regionalization of the Group and Phase Velocity

A 3-D model of the lithospheric structure is derived through a two-step inversion procedure (plus an intermediate step for taking the crust into account) [Montagner and Nataf, 1986]. First, the continuous regionalization method [Montagner, 1986] is applied to obtain the geographical distribution of the local group and phase velocities and their azimuthal terms at different periods. In the next step for inversion at depth, we simultaneously invert the Rayleigh group and phase velocities for the isotropic case to provide better constraints on the crust and the final 3-D tomographic model including azimuthal anisotropy terms derived

by perturbation theory. The method has been implemented on a regional scale for Africa [Sebai *et al.*, 2006] and Pacific plates [Montagner, 2002] and on a global scale [Beucler and Montagner, 2006; Burgos *et al.*, 2014] to derive the lithospheric and upper mantle structure.

In the framework of geometrical ray theory approximation, the local phase velocity $V(T, \theta, \phi, \psi)$ at geographical coordinates (θ, ϕ) denoted as \mathbf{r} , along a given great-circle path from the epicenter (E) to the receiver (R) can be written as

$$\frac{1}{V_i(T)} = \frac{1}{\Delta} \int_E^R \frac{1}{V(T, \theta, \phi, \psi)} ds, \quad (2)$$

where V_i is the phase (or group) velocity measurement for i th path at a given period T and Δ is the epicentral distance between the source (E) and the receiver (R) for that path.

Following the approach of Smith and Dahlen [1973], the local surface wave velocity $V(T, \mathbf{r}, \psi)$ in a weak anisotropic medium can be expressed as a Fourier series of the azimuth ψ as

$$V(T, \mathbf{r}, \psi) = \alpha_0(T, \mathbf{r}) + \alpha_1(T, \mathbf{r})\cos(2\psi) + \alpha_2(T, \mathbf{r})\sin(2\psi) + \alpha_3(T, \mathbf{r})\cos(4\psi) + \alpha_4(T, \mathbf{r})\sin(4\psi) \quad (3)$$

where T is the period of the wave and α_0 and α_i ($i = 1, 4$) are the anisotropy coefficients that describe the azimuthal dependence of the phase (or group) velocity. The term α_0 is independent of azimuth and corresponds to the azimuthally averaged velocity of the local medium that is assumed to be transversely isotropic with a vertical symmetry axis.

The least squares inversion is controlled by three parameters: (1) uncertainty in the observed phase (or group) velocity data (σ_d), (2) a priori parameter errors (σ_p) in isotropic (0.05 km s^{-1}) and anisotropic (0.01 km s^{-1}) terms that control the amplitude of the inverted 2-D perturbation model, and (3) horizontal correlation length L_{corr} (200 km; see SI Figure S3.1) which controls the horizontal smoothing using an a priori Gaussian covariance function:

$$C_o(r, r') = \sigma_p(r)\sigma_p(r') \exp\left(\frac{-\Delta_{rr'}^2}{2L_{\text{corr}}^2}\right), \quad (4)$$

where $\Delta_{rr'}$ is the distance between two geographical points. Montagner and Nataf [1986] have shown that the Rayleigh wave velocity is mainly sensitive to the 2ψ terms, whereas the Love wave velocity is mainly sensitive to the 4ψ terms. We invert for both terms to avoid any bias in the other terms in the expansion. The local phase velocities are retrieved from the regionalization method that is capable of handling large data sets [Debayle and Sambridge, 2004] but does not allow the computation of the a posteriori covariance matrix owing to heavy computational cost. The error in the regionalized velocity is computed by the bootstrapping method [Efron and Tibshirani, 1991], which provides the standard deviation of the inversion of 20 random realizations sampling 80% of the dispersion data set (Jackknife resampling).

The high-resolution regionalized dispersion perturbation maps inverted in $1^\circ \times 1^\circ$ grid with 200 km lateral resolution are presented in Figures 4 and 5, where the background reference model used is the average velocity of the data at a given period. The checker board test (see SI Figures S3.2 and S3.3) has been done for both the isotropic and anisotropic structure with the same parametrizations used in the regionalization. Our regionalized dispersion perturbation maps depict most of the geological features such as thick sediments in the Bay of Bengal, thick crust in the Himalayas and Tibetan plateau, and the high-velocity subducting Indian plate.

3.3.1. Regionalized Group Velocity Maps

The group velocity maps (Figure 4) derived from our database are in good agreement with the previous models [Ritzwoller and Levshin, 1998; Mitra *et al.*, 2006b; Acton *et al.*, 2010]. Also, consistency is seen in what we expect in both the shallow and deep structure beneath the study area. A comparison of our regionalized maps with global surface wave dispersion data set of Ekström [2011] is presented in SI Figures S3.4 and S3.5. A good agreement between both maps can be easily seen for large-scale features like slow velocities in the Himalayas and the Tibetan plateau and fast velocities in the oceans at short periods (Figure S3.4). Also, at long periods (Figure S3.5), the fast velocities in central India and their extension further north are in good

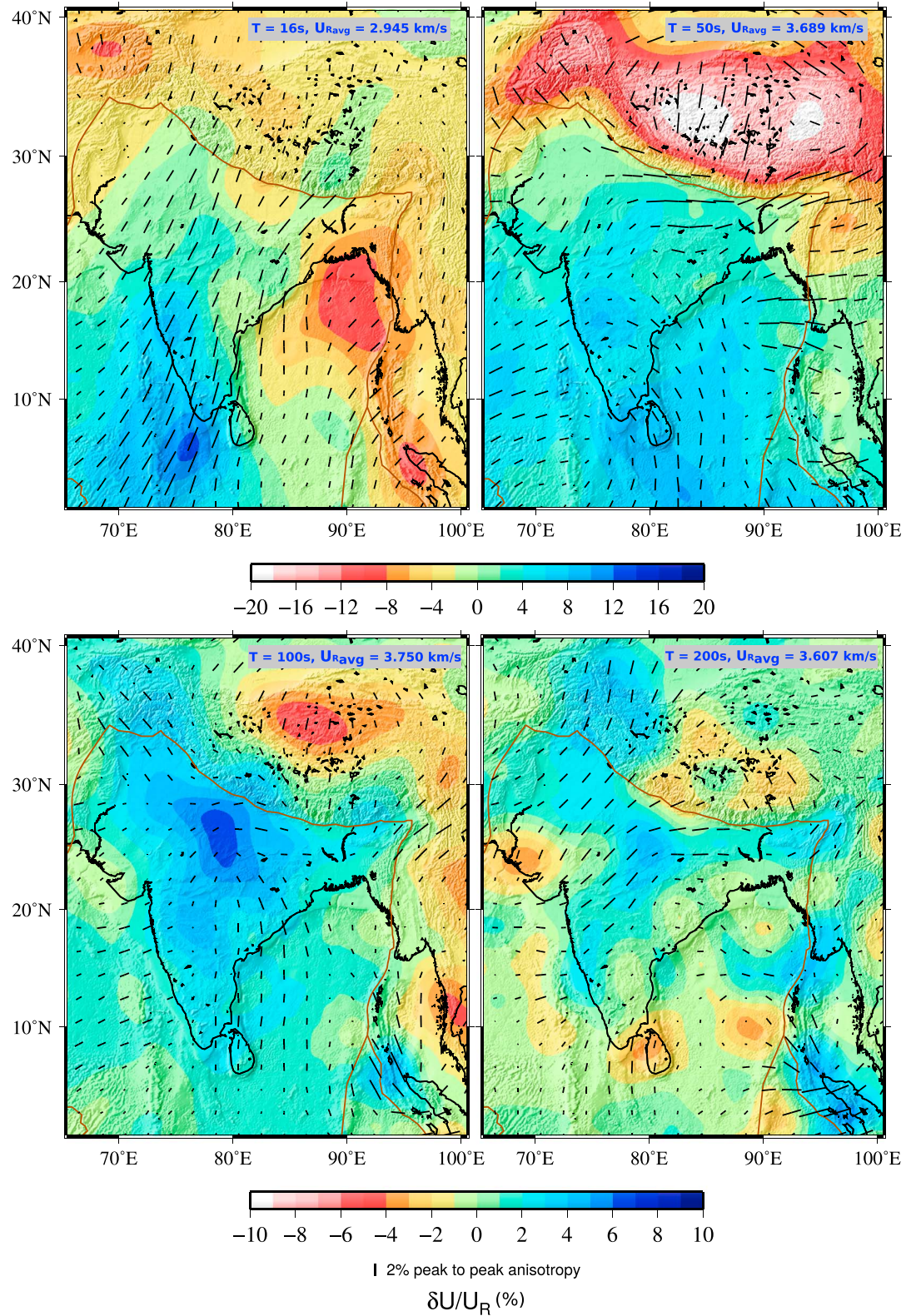


Figure 4. Rayleigh wave group velocity perturbation maps with respect to the average velocity at 16, 50, 100, and 200 s. Bars represent directions of fast axis of azimuthal anisotropy.

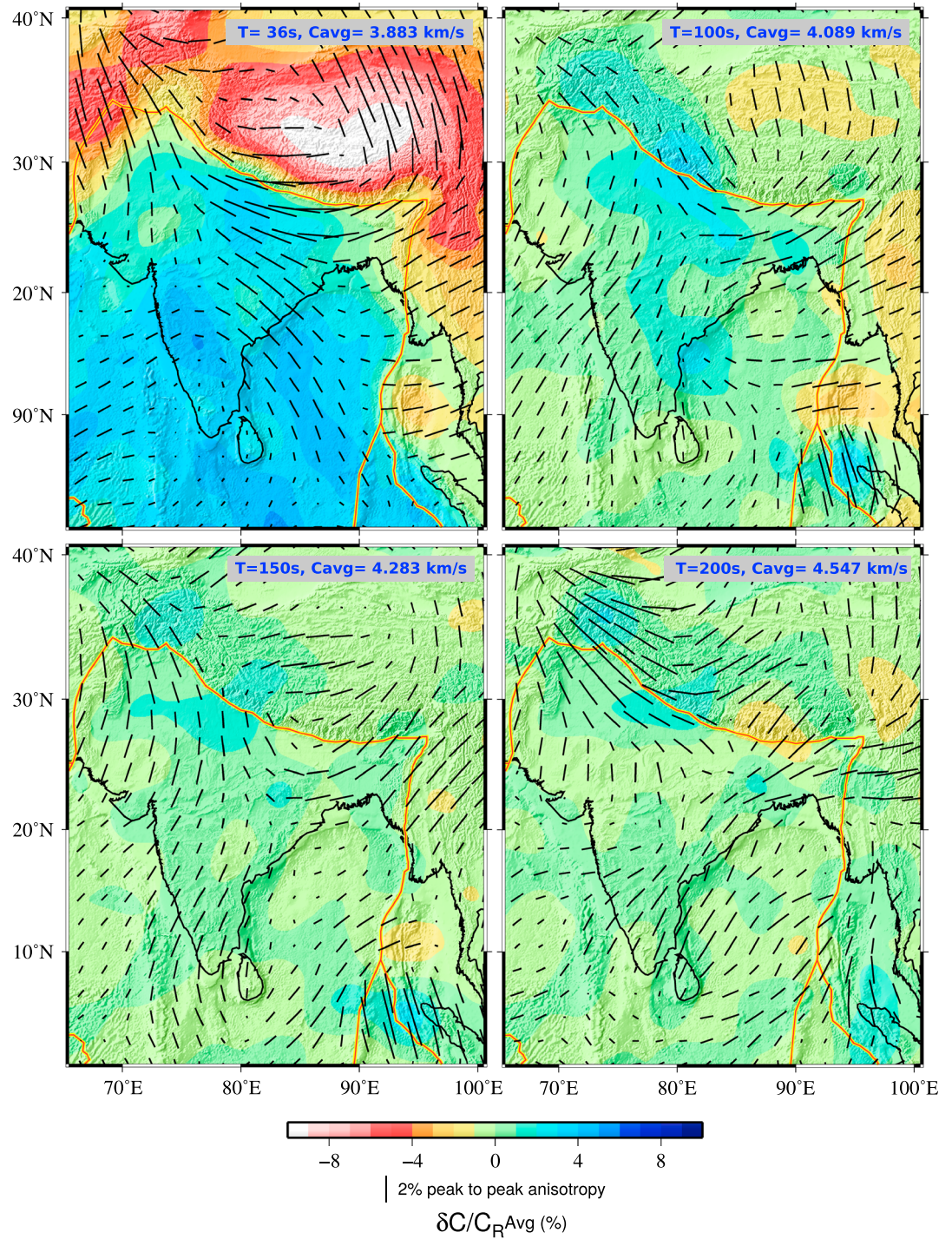


Figure 5. Rayleigh wave phase velocity perturbation maps with respect to the average velocity at 36, 100, 150, and 200 s respectively. Bars represent directions of fast axis of azimuthal anisotropy.

agreement. From our study, at short periods of 16 s, slow velocities are associated with thick sediments along the plate boundaries, the Indo-Gangetic plains, the Indo-Burman ranges, the Bay of Bengal, and the Andaman-Sumatra trench. The dominant slow velocities at 50 s are related to the thick crust in the Himalayas and the Tibetan plateau. The high-velocity anomalies between 50 and 200 s in the central part of India (CI), the Deccan Volcanic Province (DVP), and the cratonic blocks are possibly related to the Precambrian shield.

3.3.2. Regionalized Phase Velocity Maps

The phase velocity perturbation maps presented in Figure 5 are comparable with the group velocity perturbation maps (e.g., at 36 s and 100 s). Similar to the exercise we performed for the group velocity maps, we compare the phase velocity maps with those of *Ekström* [2011] in Figure S3.6. The large-scale features such as the slow anomalies in the Himalaya and Tibetan plateau are again related to a thick crust and the fast velocities are associated with the Indian Precambrian shield. At 36 s, the fast anomalies reflect the oceanic lithosphere, the continental uppermost mantle, and a good contrast along the plate boundaries (e.g., Andaman-Sumatra). The fast anomalies (e.g., 100 s in both the group/phase velocity maps) beneath central India are due to the cratonic root and those in the Indo-Gangetic plains are related to the northward underthrusting of India beneath Eurasia. The fast axis direction of azimuthal anisotropy seems more coherent within the oceans (e.g., Arabian Sea) and in most parts of the Indian shield between 100 and 150 s. The variability in the fast axis directions between 36 and 100 s, especially in the CI, DVP, and DC regions, may be due to the deformation and small-scale heterogeneities present within the lithosphere.

A few inconsistencies present in the regionalized group and phase velocity maps can be easily seen. These inconsistencies could be apparent or real (or both). The velocity kernels sample different depth ranges; the group velocity kernel (with a change of sign at depth) is more complex than the phase velocity kernel. Also, the inconsistency could be due to noise in the data and retrieval of group/phase velocities using different approaches. The final goal is to suppress the inconsistency in the dispersion data and to provide coherent maps of the study area. We show the variance reduction between data and model dispersion in SI Figure S4.1 and address these issues, and we present in SI Figures S4.2–S4.4 a regionalized data prediction from our 3-D model.

4. Inversion at Depth

While constructing tomographic images of the Earth's interior, it is important to correct for the influence of the shallow structure. Sedimentary thickness and Moho depth variations are so strong that they affect dispersion of surface waves up to at least 100 s. It has been shown [*Montagner and Jobert, 1988*] that perturbation theory is inadequate to correct for the crustal effects. In our study region, we have large variations in the crustal structure, which require a more rigorous approach to avoid any bias in the upper mantle structure. To improve the crustal and the a priori model for the anisotropic inversion at depth, we follow a two-step depth inversion. First, we simultaneously invert for the isotropic model using Rayleigh wave group and phase dispersion data. The final 3-D shear wave velocity and the fast axis anisotropy parameters are obtained by perturbation theory.

4.1. Rayleigh Wave Isotropic Inversion

A 3-D isotropic model is derived from joint inversion of group and phase velocities of Rayleigh waves using the code SWAVETRIN (*S* wave velocity transdimensional inversion) [*Haned et al., 2015*]. This method automatically adapts the model parameterization to the group or phase velocity uncertainty. The a priori Earth model is divided into $1^\circ \times 1^\circ$ cells. At each grid point, a 1-D reference model comprising the local CRUST 1.0 [*Laske et al., 2013*] on top of the Preliminary Reference Earth Model (PREM) [*Dziewonski and Anderson, 1981*] is constructed, where the 220 km discontinuity is replaced by a gradient. The *S* wave velocity model is retrieved as a weighted sum of B-spline basis functions and the local 1-D reference model. The inversion code works in two loops—an inner loop, which computes the optimum model weighting coefficients for a given spline basis by minimizing the misfit between data and synthetic velocity measurements, and an outer loop which determines the optimum spline basis to minimize the data misfit and the uncertainty in the *S* wave velocity model together. Where the model weighting coefficients are actually the model parameters, they are the coordinates of a point in model space. Synthetic group or phase velocities are computed following the approach of *Saito* [1988].

4.2. Anisotropic Inversion of Phase Velocities

In a slightly anisotropic and heterogeneous medium, the elastic coefficients C_{ij} are linear combinations of 13 (plus density) parameters [*Montagner and Nataf, 1986*]. The first five parameters (*A, C, F, L, N*) [*Love, 1927*] describe the transversely isotropic medium with a vertical symmetry axis (related to the 0ψ term). The other six parameters (*B, $\psi_B, G, \psi_G, H, \psi_H$*) are azimuthal variations of *A, L, and F* related to the 2ψ terms and the additional two parameters (*E, ψ_E*) that represent azimuthal variations of *A* or *N* are related to the 4ψ terms.

In the framework of a first-order perturbation theory, the forward problem for the Rayleigh wave phase velocity perturbation from equation (13) in *Montagner* [2007] can be rewritten as

$$\delta C_R(T) = \int_0^a \left[\begin{array}{l} \frac{\partial C_R(T)}{\partial A} (dA + B_c \cos 2\psi + B_s \sin 2\psi + E_c \cos 4\psi + E_s \sin 4\psi) + \\ \frac{\partial C_R(T)}{\partial C} dC + \frac{\partial C_R(T)}{\partial F} (dF + H_c \cos 2\psi + H_s \sin 2\psi) + \\ \frac{\partial C_R(T)}{\partial A} (dL + G_c \cos 2\psi + G_s \sin 2\psi) + \end{array} \right] \frac{dz}{\Delta h}, \quad (5)$$

where a is the radius of the Earth, Δh is a factor for normalization of thickness in the kernels, and subscripts “ c ” and “ s ” are the cosine and sine terms of azimuthal anisotropy. Partial derivatives of phase velocity ($\partial C_R / \partial P_i$) are calculated based on the formalism of *Takeuchi and Saito* [1972] and those of group velocities ($\partial U_R / \partial P_i$) are constructed from the partial derivatives of phase velocities following *Rodi et al.* [1975]. In the study area, at every geographical grid point (θ, ϕ), the partial derivatives are constructed using the 1-D reference starting model obtained from the isotropic inversion.

The anisotropy depth inversion method [*Montagner and Nataf*, 1986] is based on the least squares inverse algorithm of *Tarantola and Valette* [1982], which handles slightly nonlinear problems. The inversion scheme provides an a posteriori model with its error bars for a given data set. The Earth model relates the model parameters and the a priori model with its covariance matrix. The important constituents of the inversion scheme are uncertainties in the data and model parameters and design of the covariance matrix of parameters [*Montagner and Anderson*, 1989]. The data errors computed from the regionalization step are taken into account in the inversion at depth, and the final errors in the parameters are estimated by the diagonal terms of the a posteriori covariance matrix. The Gaussian vertical correlation lengths introduced in the inversion increase with depth from 20 to 40 km. The best resolved parameters from the database are the shear wave velocity (V_{SV}), amplitude (G) and direction (ψ_G) of the fast axis azimuthal SV wave anisotropy. An example is presented in SI Figure S4 for isotropic and anisotropic inversions at depth and the corresponding resolved model parameters (profile located close to HYB GEOSCOPE seismic station; see in SI Figure S5.2). We present only V_{SV} , G , and ψ_G parameters in the 3-D model (Figure 6) as derived from the perturbation theory. Our 3-D tomography model well predicts the data, and it can be easily seen for isotropic term in SI Figures S4.2 and S4.3 and anisotropic term in Figure S4.4. In our tomographic model, all the regional-scale tectonic structures down to 60 km depth have been well resolved. The slow velocities in the Himalayas and the Tibetan plateau correspond to the thick crust, whereas the fast velocities correspond to the Indian plate subducting along the plate boundary. Significant velocity contrast is observed in the oceanic regions, between the older Bay of Bengal in the east and the younger Arabian Sea in the west. At larger depths (>100 km), a clear demarcation of ocean continent boundary can be seen in the velocity anomaly maps. In the northwest of the study region, the high-velocity present at large depth (>100 km) indicates the ongoing subduction of the Indian continental lithosphere under Hindu-Kush and Pamir regions. Similar observations of high-velocity anomalies trending NW-SE along the collision boundary were made from the global body wave tomographic models [*Replumaz et al.*, 2010, 2014; *Singh et al.*, 2014]. In the SI Figure S6, we have discussed and compared our shear wave velocity model with four other global tomographic models. The shear velocity perturbation maps of global models are presented in Figure S6.2. Compared to our model, these global models seem to be consistent with the large-scale features. For example, at a depth of 100 km, a fast velocity anomaly is seen in IGP. Further, at 150 km and 200 km depths fast velocity anomalies are observed in central Indian India and plate boundaries in the north. The discrepancy between our model and the global models and among the global models themselves stem from varied data coverage, data types (e.g., waveforms, body waves, or surface waves), and the tomographic methods adopted. As a general rule, the amplitudes of seismic anomalies are not well constrained. Our fast axis of azimuthal anisotropy (ψ_G) directions at a particular depth seem coherent with the tectonic units such as the Arabian sea (at 60 km in the NE-SW direction), Bay of Bengal (at 100 and 150 km along NS direction), Tibetan plateau (NS at 150 km depth), and variations along the plate boundaries of the continents (e.g., IGP and Himalayas). We only discuss here the isotropic parameter of our tomographic model and anisotropy parameters are presented in SI Figure S5 to demonstrate that the account of anisotropy does not significantly affect the interpretation of isotropic model.

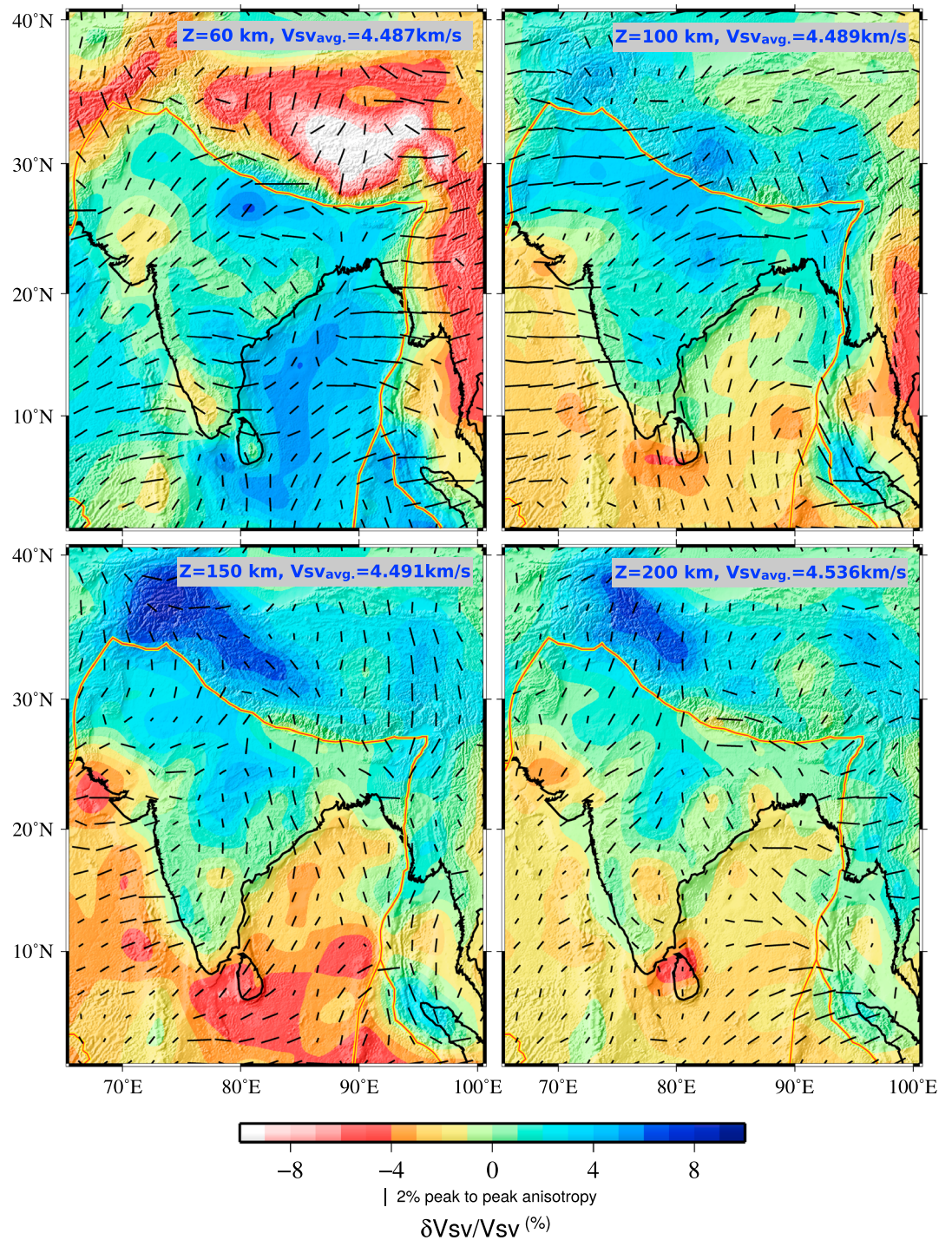


Figure 6. Seismic velocity (V_{sv}) perturbation maps with respect to the average model at 60, 100, 150, and 200 km depths. The azimuths of fast axes of anisotropy (ψ_G) are shown as bars.

5. Lithospheric Model for Different Blocks

Characterizing the Lithosphere-Asthenosphere boundary (LAB) beneath continents is important to understand its geodynamic evolution. However, the definition of this boundary varies according to the geophysical observations [e.g., Eaton et al., 2009]. In seismic tomography, the LAB can be obtained from the parameters derived from inversion of surface wave dispersion data. Since surface waves are sensitive to long wavelength

lateral variations, they only see a filtered version of the discontinuity. The LAB can be defined as the maximum of the gradient ($-\partial V_{sv}/\partial z$) above the low velocity zone [Burgos *et al.*, 2014]. In general, cratons are stable and undeformed since Archean. The base of the craton is cooler compared to that beneath other tectonic regions. The seismic velocity contrast across the LAB is not unequivocally observed beneath cratonic blocks, in contrast to a sharp one beneath the oceanic lithosphere. Hence, the maximum of gradient is not so evident beneath continents due to the nonexistence of a sharp boundary between the lithosphere and asthenosphere (see SI Figure S5.1). We can interpret the LAB as a drop in seismic velocity in the lithosphere ($\Delta V_{sv}/V_{sv} > P_o$, where P_o is the positive anomaly). We used the perturbation cutoff P_o ($>1.25\%$) to obtain the depth of the LAB and present vertical cross-section profiles which show the LAB beneath different blocks and also the presence of low velocity layers within the lithosphere, in Figures 7 and 8. A detailed 3-D model of the shear velocity structure down to the lithospheric level beneath the Indian shield derived from surface wave data can be seen in Figures 6–8. We discuss the results for each of the major geological units and various cratonic blocks in the study area.

5.1. Southern Granulite Terrain (SGT)

The Southern Granulite Terrain (Figure 1) has a complex crustal and lithospheric structure owing to various shear and tectonically disturbed zones [Behera, 2011]. In Figure 7, the cross section H1-H2 depicts an oceanic lithosphere in the southern end of Indian continent. Towards further north, in cross section H3-H4, two layer anomalies (Q1 and S1) within the continent are observed, flanked on both sides by the oceanic asthenosphere. The slow velocity anomalies (60–80 km marked as Q1) near the west coast of south India in Figure 6 (also seen in Figure 7: V3-V4 and Figure 8: X3-X4) are probably related with plume activity in the past (e.g., Marion and Reunion) [Torsvik *et al.*, 1998; O'Neill *et al.*, 2003]. During ~90–130 Ma, the head of the Marion plume was present beneath the southwestern part of the Indian lithosphere and played an important role in the opening of the Indian Ocean between India and Madagascar [Storey and Mahoney, 1995; Raval and Veeraswamy, 2003a; Torsvik *et al.*, 2013]. The plume effect continued till ~65 Ma due to the Reunion hot spot. The plume beneath a thick lithosphere may not have enough strength to easily break the continent, but it may alter the lithosphere (e.g., Q1). At a similar depth, the oceanic Lithosphere Asthenosphere Boundary is observed as a slow anomaly(Q1), which seems linked with the LAB depth under the continental lithosphere. Ray [2003] suggested that the structure beneath this area and in other preexisting weak zones such as shear/suture zones between the Dharwar Craton and Southern Granulite Terrain might be related to the “mantle heat flow.” Beneath the Q1 anomaly, we observed moderate high-velocity anomalies (~1.25%) clearly separated from the oceanic asthenosphere (Figure 7: H3-H4 and V3-V4) and possibly related to the paleolithospheric root. The fast axis has an east-west direction (Figure 6) at shallow depths (60–100 km) and close to north south (NNE-SSW) at deeper depths.

5.2. Dharwar Craton (DC)

The Dharwar Craton is separated into the eastern and western parts by the Closepet Granite (CG) (Figure 1). The Eastern Dharwar Craton (EDC) was formed in the late Archean (~2.7 Ga) and hosts the middle to late Proterozoic Cuddapah basin (CB). The Western Dharwar Craton (WDC) was formed much earlier, in the Archean (~3.6 Ga). Significant differences are observed in the crustal and upper mantle structure of these two blocks. The WDC crust is 10–15 km thicker, with a predominantly mafic composition as suggested from surface wave dispersion [Borah *et al.*, 2014a, 2014b] and receiver function studies [Gupta, 2003; Kiselev *et al.*, 2008]. Beneath the WDC, we observe a thick (~50 km) slow velocity layer (Figure 7: H5-H6 and V1-V2 and Figure 8: X3-X4) at around 50–100 km depth and a thick lithosphere with the presence of ~2% faster velocity down to ~160 km. Compared to the WDC, the lithosphere beneath the EDC is almost flat and thinner (~120 km), without any presence of slow velocity within it.

The lithospheric model presented by Bodin *et al.* [2013] from joint inversion of receiver function and surface waves from HYB seismic station in the EDC suggests a MLD at ~100 km and LAB at ~150–200 km. Our model (vertical profile in SI Figure S4 also in Figure 8 X3-X4) does not reveal a thick lithosphere. The area is surrounded by different tectonic units and located on EDC and not far from WDC (as seen in Figure S5.2). Although, they find a shallow LAB (~100 km) from receiver functions, after joint inversion with surface wave data (Rayleigh waves data taken from Ekström [2011]), they find a deeper LAB (~150–200 km). The lateral resolution of surface waves is ~600 km in Ekström [2011] model and only one station on the Indian shield makes the resolution even worse. One possible reason is the lack of resolution at depth when different kinds

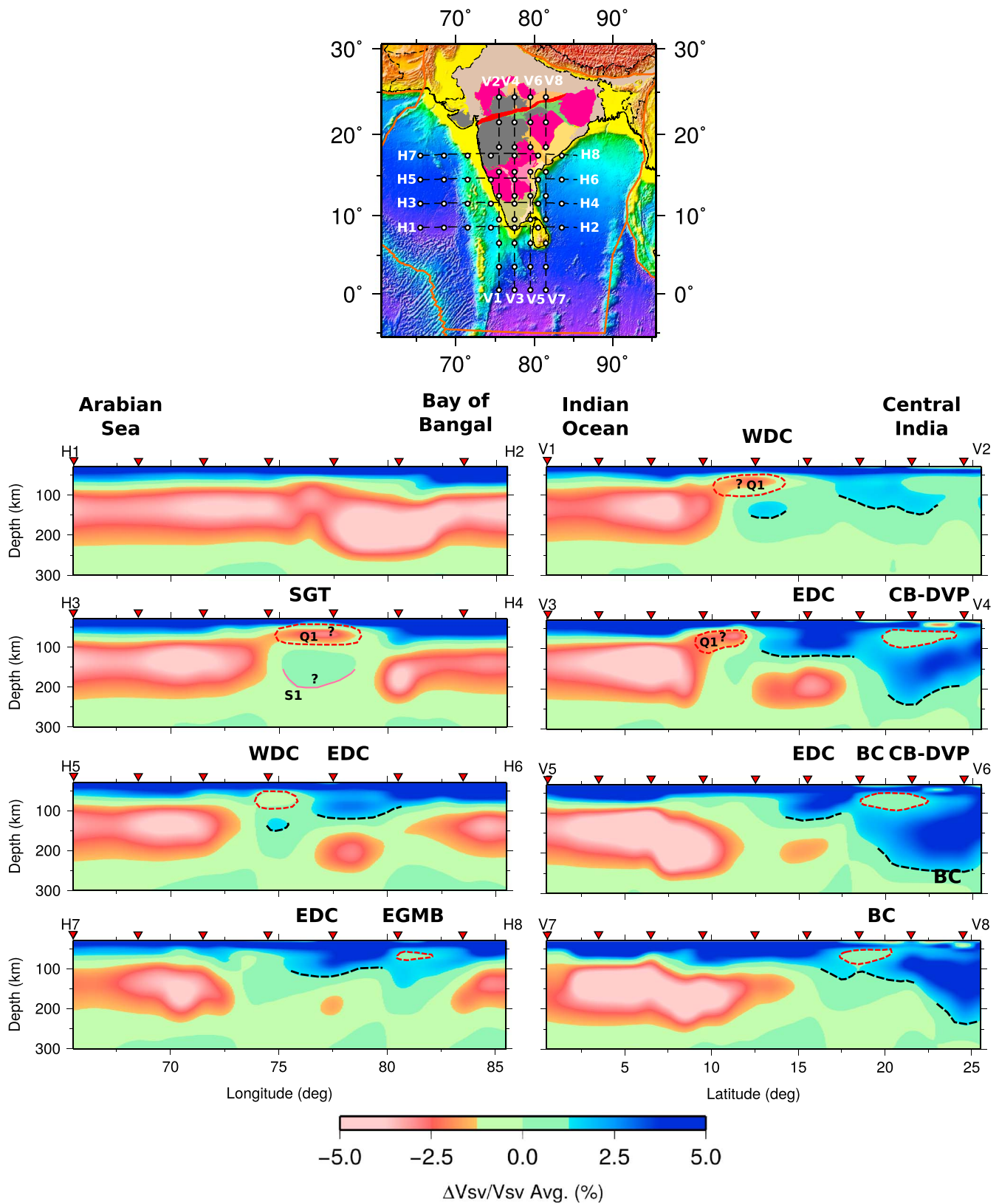


Figure 7. Shear wave (V_{sv}) velocity perturbations along west-east profiles H1-H2, H3-H4, H5-H6, and H7-H8 and south-north profiles V1-V2, V3-V4, V5-V6, and V7-V8 shown in the map, along with the Indian cratons. In each panel, the black dotted lines denote the interpreted LAB boundary and slow velocities are shown by red dots within the lithosphere.

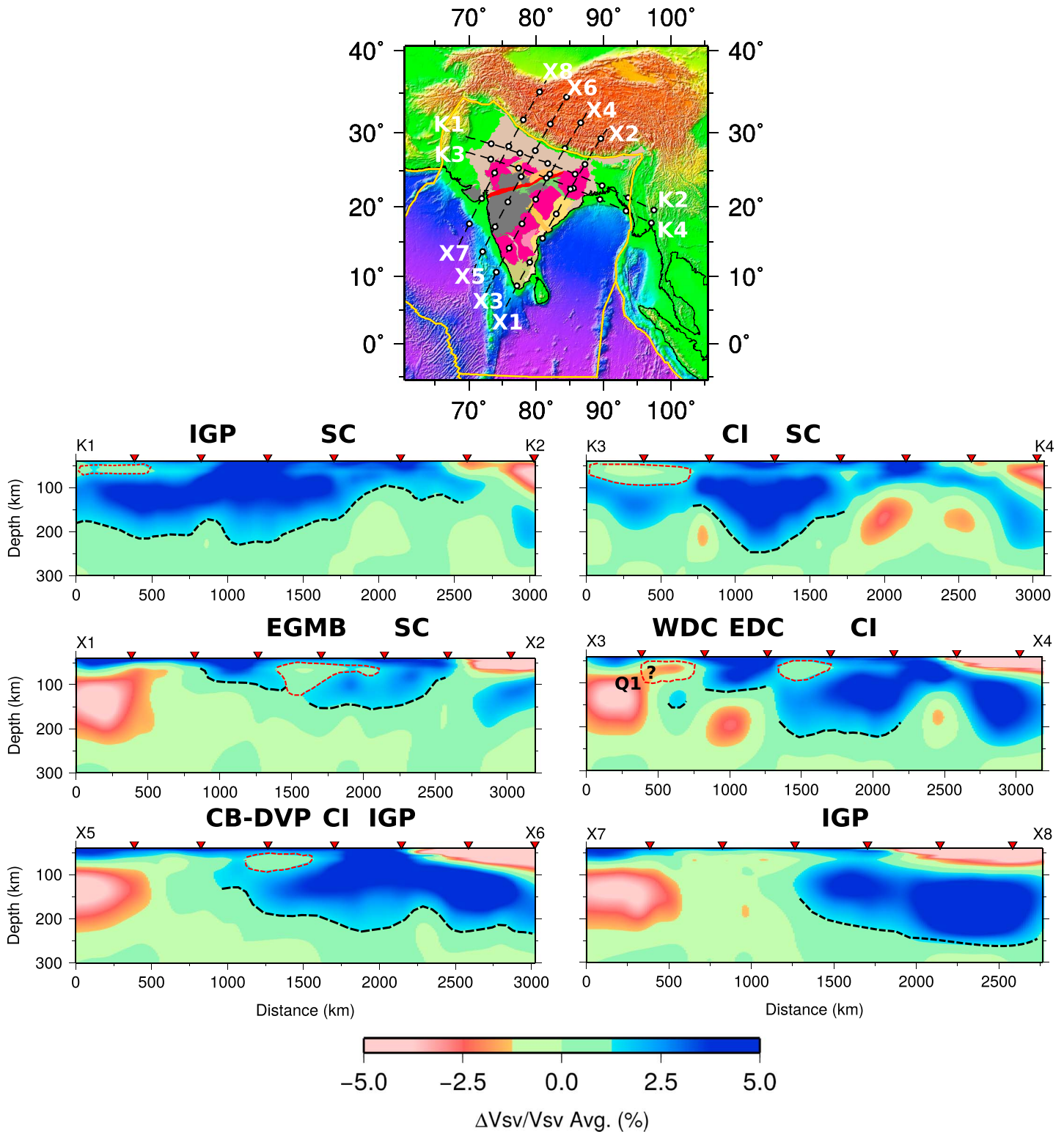


Figure 8. Shear wave (V_{sv}) velocity perturbations along oblique profiles X1-X2, X3-X4, X5-X6 and X7-X8 and K1-K2 and K3-K4 shown in the map along with the Indian cratons. In each panel, the black dotted lines denote the interpreted LAB boundary and slow velocities are shown by red dots within the lithosphere.

Table 1. Lithospheric Thickness of the Major Cratonic Blocks in the Indian Shield Along With the Respective Slow Velocity Layer Indications Within the Lithosphere^a

Cratonic Block	Lithospheric Thickness ± 30 (in km)	Sublithospheric Low Velocity Zone
Easter Dharwar Craton (EDC)	120	No
Western Dharwar Craton (WDC)	160	Yes
Bastar Craton (BC)	140–200	Yes
Singhbhum Craton (SC)	160–200	Yes
Bundelkhand Craton (BhC or CI)	200–250	Yes
Craton beneath DVP (CB-DVP)	150–200	Yes

^aThe corresponding average shear wave velocity profile is presented in Figure S5.3.17.

of data sets are used. Another reason is the complexity of the lithospheric structure with at least two different layers in the first 250 km and the rapid change in lateral structures of cratons. As we show in our model, the thickness of lithosphere in most parts of the cratons is larger than 140 km, and the surface wave data of *Ekström* [2011] cannot resolve these small-scale (~ 350 km) cratonic blocks. These small cratons (EDC and WDC) are averaged at large wavelength. That is, the reason why they only see the average thickness of the Indian craton but not the regional, small-scale variations in cratonic thicknesses.

5.3. Central India (CI)

The cratons including the Bastar (BC), Singhbhum (SC), and Bundelkhand (BhC) along with the Deccan Volcanic Province (DVP) (Figure 1) can be grouped as the central Indian shield. Our results reveal a thick cratonic lithosphere in Central India having a large variability from 150 km in the east and west to ~ 250 km in the central part. For the Bastar Craton, the thickness of lithosphere varies between the eastern (~ 140 km, Figure 7: V7-V8) and western parts (~ 200 km, Figure 7: V5-V6). The observations beneath the Singhbhum Craton reveal a thick lithosphere (Figure 8: K1-K2, K3-K4, and X1-X2 cross section), where the lithosphere is ~ 160 km in the east and ~ 200 km in the west. The lithospheric boundaries for Bastar and Singhbhum cratons seem to have a strong gradient toward the central part. The boundary between central and western cratonic blocks is not so clear. In the DVP region, the lithospheric roots are deep toward the centre of the continent. The thickest lithosphere in India (~ 250 km; Figure 7: V3-V4) is, however, seen along a NE-SW direction cutting across central India (Figure 6), which is a significant observation. The LAB beneath the DVP shows large variations (Figure 8: X5-X6) being at a depth of 160 km in the southwest (Figure 7: H7-H8 and V1-V2) and 250 km in the northeast portions (Figure 7: V3-V4). A new observation that emerges from our results in this region is the fast velocity and deep roots revealing the cratonic lithosphere in the central region, where most of the surface is covered by sediments (Figures 6 and 8: K3-K4). In Figure 6, at 60 km, the small moderate positive velocity in the western and southern parts of the DVP is also present in the cross sections (Figure 7: V3 to V6 and Figure 8: X3 to X8), highlighted as red dots is slow velocity within the lithosphere. Above, the surface is covered by large volcanic eruptions around ~ 65 Ma. The slow velocity could be related to large-scale deformation in this area. The lithospheric roots are not so clear around this region.

5.4. Indo-Gangetic Plain (IGP) and Himalaya

In the Indo-Gangetic plain (IGP) with most of the region covered by the Indo-Gangetic sediments and minor basin, we find a 200–250 km thick lithosphere (Figure 8: K1-K2, X3-X4, X5-X6, and X7-X8). We observe a lateral velocity contrast between the north and south across Himalaya and the thickness also increases from east to west along the plate boundary (Figure 6: at depth 150 and 200 km and Figure 8: X1 to X8). The high-velocity region beneath IGP and the Himalayas shows the Indian lithosphere underthrusting beneath Eurasia.

6. Discussion

Our model shows several continental roots beneath the cratons varying between 120 and 250 km depths (Table 1), consistent with the geochemistry/petrological analysis [*Babu et al.*, 2009; *Griffin et al.*, 2009] and the recent heat flux data [*Roy and Mareschal*, 2011]. However, a velocity decrease in the depth range of ~ 80 – 100 km found from receiver functions [*Kumar et al.*, 2007, 2013] and previously interpreted as the base of a thin lithosphere could well be the midlithospheric discontinuity (MLD) [*Abt et al.*, 2010; *Yuan and Romanowicz*, 2010; *Yuan et al.*, 2011]. In our study, we have shown (Figure 6) that the uppermost mantle

velocity drop occurs around 60 km in the central as well as the southern portions of the continent compared to 100 km. We highlight such velocity reductions in our model within the different cratonic blocks. A similar velocity drop is also seen beneath other cratonic regions from global [Lekic and Romanowicz, 2011] and regional studies for the eastern European cratons [Nita et al., 2016]. We observed a velocity reduction ($\sim 1\text{--}2\%$) within the lithosphere beneath the DVP and most of the cratonic blocks. A few recent studies [e.g., Wirth and Long, 2010; Karato et al., 2015] discussed in detail about the possible reasons behind such velocity drops at the MLD. A subsequent study of receiver functions [Kumar et al., 2013] found MLD and LAB below a large number of stations, but the interpretation is probably nonunique and a careful analysis is required to interpret MLD and LAB especially when the medium is heterogeneous and anisotropic [e.g., Wölbern et al., 2012; Sodoudi et al., 2013].

Another model of the Indian lithosphere and upper mantle was recently obtained from body wave (P and S) travel time tomography [Singh et al., 2014] with quite a good data coverage. The body waves have a better resolution, but the ray coverage in the uppermost mantle is poor. Velocity models from body wave tomography bring out the heterogeneous nature of the mantle beneath India and seem to favor the deep lithospheric roots. However, they are unable to quantify the thickness of the different cratonic blocks, the midlithospheric discontinuity, and most of the detailed layering in the cratonic regions like DVP, WDC, and EDC. Also, in teleseismic tomography, an a priori model designed from the global crustal model (CRUST 2.0) [Bassin et al., 2000] with a 1-D model of the upper mantle may not be a good starting model. This may impose severe constraints on the accurate determination of the lithospheric structure. Also the deep structure down to ~ 300 km [Rawlinson et al., 2010; Obrebski et al., 2011] cannot be resolved from body waves due to lack of path coverage and most importantly without a high-resolution a priori model.

The lithospheric models presented by Kumar et al. [2007, 2013] using receiver functions and Singh et al. [2014] using body waves tomography support alterations of the Indian lithosphere due to mantle attrition processes such as plume interaction, fast drifting toward north, and continental collision between India and Asia. We also observe slow velocity anomalies at shallow depths (60 km in Figure 6 and red dots in Figures 7 and 8) and within the lithosphere, mostly in the western and southern cratonic blocks. Our model also suggests that the Archean lithosphere is prone to deformation, but the deep lithospheric roots are still present in our model. Deformation in the lithosphere could be explained by the interaction of the plumes (e.g., Kerguelen, Marion, and Reunion) and lithosphere along the weak regions of the uppermost mantle such as mobile belts and suture zones [Anderson et al., 1992] when the plume head resides beneath the continent. In our tomography model, we image the thickest lithosphere (~ 250 km) in the central part of the Indian continent which could be the keel that enables fast motion of the Indian plate. The fast axis of azimuthal anisotropy along selected profiles (SI Figure S5.1) and the respective gradient of average velocity beneath different cratonic blocks reveal a change in the fast axis anisotropy from EW to NS within the lithosphere, but it needs further analysis to correlate the two parameters (V_{sv} and ψ_G). In the present paper, we only showed the isotropic observations but did not discuss in detail the nature of these discontinuities. Additional parameters such as radial and azimuthal anisotropies would enable us to understand such boundaries and to discriminate between competing models, which shall be presented in another paper.

7. Conclusions

The 3-D tomography model of the Indian continent reflects the various geological units and cratonic blocks with high fidelity. The Lithosphere-Asthenosphere boundary (LAB) and presence of a low velocity layer within the lithosphere beneath the diverse tectonic units are also retrieved with large variability. These slow velocities are present, mostly in the southern and western part of the cratonic units, partially in the Central part of the continent and the Indo-Gangetic plains and are not so evident in the EDC.

The following important observations emerge from the study of the lithospheric structure beneath the Indian continent:

1. Our 3-D model delineates the different cratonic blocks and has a good lateral resolution ($\sim 200\text{--}300$ km).
2. Large variability in topography is observed at the Lithosphere-Asthenosphere boundary, especially in the South (DC and CB-DVP) and the central Indian continent.
3. The lithospheric thickness beneath cratons varies between 120 and 250 km.

4. The fast axis direction of the azimuthal anisotropy ψ_G has an important connection with respect to the LAB geometry beneath the cratonic blocks and also in delimiting the anisotropy parameters. More details shall be dealt in a future paper.
5. A lithospheric keel (~250 km) comprising deep cratonic roots oriented NE-SW in central India is proposed. This might play an important role for the long journey of the Indian plate after separation from the Gondwanaland.

Acknowledgments

Seismic data for the global stations are gathered from IRIS-DMC. We thank RESIF RHUM-RUM, IMD, NGRI, and IITB project teams for sharing the publicly restricted data. All the figures are generated using GMT [Wessel and Smith, 1995]. This work has been supported by a grant from the CEFIPRA project (4704-1). We thank Prakash Kumar for the suggestions and important remarks in the discussion.

References

- Abt, D. L., K. M. Fischer, S. W. French, H. A. Ford, H. Yuan, and B. Romanowicz (2010), North American lithospheric discontinuity structure imaged by P_s and S_p receiver functions, *J. Geophys. Res.*, *115*, B09301, doi:10.1029/2009JB006914.
- Acton, C. E., K. Priestley, V. K. Gaur, and S. S. Rai (2010), Group velocity tomography of the Indo-Eurasian collision zone, *J. Geophys. Res.*, *115*, B12335, doi:10.1029/2009JB007021.
- Anderson, D. L., T. Tanimoto, and Y. S. Zhang (1992), Plate tectonics and hotspots: The third dimension, *Science*, *256*(5064), 1645–51, doi:10.1126/science.256.5064.1645.
- Babu, E., Y. J. Bhaskar Rao, D. Mainkar, J. K. Pashine, and S. R. Rao (2009), Mantle xenoliths from the Kodamali kimberlite pipe, Bastar Craton, Central India: Evidence for decompression melting and crustal contamination in the mantle source, *Geochim. Cosmochim. Acta Suppl.*, *73*(13), A66.
- Bassin, C., G. Laske, and G. Masters (2000), The current limits of resolution for surface wave tomography in North America, *Eos Trans. AGU*, *81*, F897.
- Behera, L. (2011), Crustal tomographic imaging and geodynamic implications toward south of Southern Granulite Terrain (SGT), India, *Earth Planet. Sci. Lett.*, *309*(1), 166–178, doi:10.1016/j.epsl.2011.04.033.
- Beucler, E., and J.-P. Montagner (2006), Computation of large anisotropic seismic heterogeneities (CLASH), *Geophys. J. Int.*, *165*(2), 447–468, doi:10.1111/j.1365-246X.2005.02813.x.
- Beucler, E., E. Stutzmann, and J.-P. Montagner (2003), Surface wave higher-mode phase velocity measurements using a roller-coaster-type algorithm TL - 155, *Geophys. J. Int.*, *155*, 289–307, doi:10.1046/j.1365-246X.2003.02041.x.
- Bhattacharya, S. N. (1974), The crust-mantle structure of the Indian Peninsula from surface wave dispersion, *Geophys. J. R. Astron. Soc.*, *36*(2), 273–283, doi:10.1111/j.1365-246X.1974.tb03639.x.
- Bhattacharya, S. N. (1981), Observation and inversion of surface wave group velocities across Central India, *Bull. Seismol. Soc. Am.*, *71*(5).
- Bodin, T., H. Yuan, and B. Romanowicz (2013), Inversion of receiver functions without deconvolution—Application to the Indian Craton, *Geophys. J. Int.*, *196*, 1025–1033, doi:10.1093/gji/ggt431.
- Borah, K., S. S. Rai, K. Priestley, and V. K. Gaur (2014a), Complex shallow mantle beneath the Dharwar Craton inferred from Rayleigh wave inversion, *Geophys. J. Int.*, *198*(2), 1055–1070, doi:10.1093/gji/ggu185.
- Borah, K., S. S. Rai, K. S. Prakasam, S. Gupta, K. Priestley, and V. K. Gaur (2014b), Seismic imaging of crust beneath the Dharwar Craton, India, from ambient noise and teleseismic receiver function modelling, *Geophys. J. Int.*, *197*(2), 748–767, doi:10.1093/gji/ggu075.
- Boschi, L., and G. Ekström (2002), New images of the Earth's upper mantle from measurements of surface wave phase velocity anomalies, *J. Geophys. Res.*, *107*(B4), 2059, doi:10.1029/2000JB000059.
- Burgos, G., J.-P. Montagner, E. Beucler, Y. Capdeville, A. Mocquet, and M. Drilleau (2014), Oceanic Lithosphere-Asthenosphere boundary from surface wave dispersion data, *J. Geophys. Res. Solid Earth*, *119*, 1079–1093, doi:10.1002/2013JB010528.
- Debayle, E., and M. Sambridge (2004), Inversion of massive surface wave data sets: Model construction and resolution assessment, *J. Geophys. Res.*, *109*, B02316, doi:10.1029/2003JB002652.
- DeMets, C., R. G. Gordon, D. F. Argus, and S. Stein (1990), Current plate motions, *Geophys. J. Int.*, *101*, 425–478, doi:10.1111/j.1365-246X.1990.tb06579.x.
- Dziewonski, A. M., and D. L. Anderson (1981), Preliminary reference Earth model, *Phys. Earth Planet. Inter.*, *25*(4), 297–356, doi:10.1016/0031-9201(81)90046-7.
- Dziewonski, A. M., T.-A. Chou, and J. H. Woodhouse (1981), Determination of earthquake source parameters from waveform data for studies of global and regional seismicity, *J. Geophys. Res.*, *86*, 2825, doi:10.1029/JB086iB04p02825.
- Eaton, D. W., F. Darbyshire, R. L. Evans, H. Grütter, A. G. Jones, and X. Yuan (2009), The elusive Lithosphere-Asthenosphere boundary (LAB) beneath cratons, *Lithos*, *109*(1), 1–22, doi:10.1016/j.lithos.2008.05.009.
- Efron, B., and R. Tibshirani (1991), Statistical data analysis in the computer age, *Science*, *253*(5018), 390–5, doi:10.1126/science.253.5018.390.
- Ekström, G. (2011), A global model of Love and Rayleigh surface wave dispersion and anisotropy, 25–250 s, *Geophys. J. Int.*, *187*(3), 1668–1686, doi:10.1111/j.1365-246X.2011.05225.x.
- Ferreira, A. M. G., J. H. Woodhouse, K. Visser, and J. Trampert (2010), On the robustness of global radially anisotropic surface wave tomography, *J. Geophys. Res.*, *115*, B04313, doi:10.1029/2009JB006716.
- Fouch, M. J., and S. Rondenay (2006), Seismic anisotropy beneath stable continental interiors, *Phys. Earth Planet. Inter.*, *158*(2–4), 292–320, doi:10.1016/j.pepi.2006.03.024.
- Griffin, W. L., A. F. Kobussen, E. V. S. S. K. Babu, S. Y. O'Reilly, R. Norris, and P. Sengupta (2009), A translithospheric suture in the vanished 1-Ga lithospheric root of South India: Evidence from contrasting lithosphere sections in the Dharwar Craton, *Lithos*, *112*, 1109–1119, doi:10.1016/j.lithos.2009.05.015.
- GSI and ISRO (1994), Project Vasundhara: Generalized geological map (scale 1:2 million), *Geol. Surv. India Indian Sp. Res. Orgn., Bangalore*.
- Gupta, S. (2003), The nature of the crust in southern India: Implications for Precambrian crustal evolution, *Geophys. Res. Lett.*, *30*(8), 1419, doi:10.1029/2002GL016770.
- Haned, A., E. Stutzmann, M. Schimmel, S. Kiselev, A. Davaille, and A. Yelles-Chaouche (2015), Global tomography using seismic hum, *Geophys. J. Int.*, *204*(2), 1222–1236, doi:10.1093/gji/ggv516.
- Karato, S., T. Ologboji, and J. Park (2015), Mechanisms and geologic significance of the mid-lithosphere discontinuity in the continents, *Nat. Geosci.*, *8*(June), 509–514, doi:10.1038/ngeo2462.
- Kiselev, S., L. Vinnik, S. Oreshin, S. Gupta, S. S. Rai, A. Singh, M. R. Kumar, and G. Mohan (2008), Lithosphere of the Dharwar craton by joint inversion of P and S receiver functions, *Geophys. J. Int.*, *173*(3), 1106–1118, doi:10.1111/j.1365-246X.2008.03777.x.
- Klootwijk, C. T., J. S. Gee, J. W. Peirce, G. M. Smith, and P. L. McFadden (1992), An early India-Asia contact: Paleomagnetic constraints from Ninetyeast Ridge, ODP Leg 121, *Geology*, *20*(May), 395–398, doi:10.1130/0091-7613(1992)020<0395:AEIACP>2.3.CO;2.

- Kumar, P., X. Yuan, M. R. Kumar, R. Kind, X. Li, and R. K. Chadha (2007), The rapid drift of the Indian tectonic plate, *Nature*, 449(7164), 894–897, doi:10.1038/nature06214.
- Kumar, P., M. Ravi Kumar, G. Sriyjanthi, K. Arora, D. Srinagesh, R. K. Chadha, and M. K. Sen (2013), Imaging the Lithosphere-Asthenosphere boundary of the Indian plate using converted wave techniques, *J. Geophys. Res. Solid Earth*, 118, 5307–5319, doi:10.1002/jgrb.50366.
- Laske, G., G. Masters, Z. Ma, and M. Pasyanos (2013), Update on CRUST1.0—A 1-degree global model of Earth's crust, in *EGU General Assembly Conference Abstracts*, vol. 15, p. 2658.
- Lekic, V., and B. Romanowicz (2011), Tectonic regionalization without a priori information: A cluster analysis of upper mantle tomography, *Earth Planet. Sci. Lett.*, 308(1–2), 151–160, doi:10.1016/j.epsl.2011.05.050.
- Levshin, A. L., T. B. Yanovskaya, A. V. Lander, B. G. Bukchin, M. P. Barmin, L. I. Ratnikova, and E. N. Its (1989), in *Seismic Surface Waves in Laterally Inhomogeneous Earth*, edited by V. I. Keilis-Borok, Kluwer, Norwell, MA.
- Love, A. E. H. (1927), *A treatise on the mathematical theory of elasticity*, 4th ed., Cambridge Univ. Press, Cambridge.
- Marone, F., and B. Romanowicz (2007), Non-linear crustal corrections in high-resolution regional waveform seismic tomography, *Geophys. J. Int.*, 170, 460–467, doi:10.1111/j.1365-246X.2007.03399.x.
- McKenzie, D. P., and J. G. Sclater (1971), The evolution of the Indian Ocean since the Late Cretaceous, *Geophys. J. R. Astron. Soc.*, 25, 437–528, doi:10.1038/scientificamerican0573-62.
- Meert, J. G., M. K. Pandit, V. R. Pradhan, J. Banks, R. Sirianni, M. Stroud, B. Newstead, and J. Gifford (2010), Precambrian crustal evolution of Peninsular India: A 3.0 billion year odyssey, *J. Asian Earth Sci.*, 39(6), 483–515, doi:10.1016/j.jseas.2010.04.026.
- Mitra, S., K. F. Priestley, V. K. Gaur, and S. S. Rai (2006a), Shear-wave structure of the south Indian lithosphere from Rayleigh wave phase velocity measurements, *Bull. Seismol. Soc. Am.*, doi:10.1785/0120050116.
- Mitra, S., K. Priestley, V. K. Gaur, S. S. Rai, and J. Haines (2006b), Variation of Rayleigh wave group velocity dispersion and seismic heterogeneity of the Indian crust and uppermost mantle, *Geophys. J. Int.*, 164(1), 88–98, doi:10.1111/j.1365-246X.2005.02837.x.
- Montagner, J. (1986), Regional three-dimensional structures using long-period surface waves, *Ann. Geophys.*, 4, 283–294.
- Montagner, J., and D. Anderson (1989), Petrological constraints on seismic anisotropy, *Phys. Earth Planet. Inter.*, 54, 82–105.
- Montagner, J. P. (2002), Upper mantle low anisotropy channels below the Pacific Plate, *Earth Planet. Sci. Lett.*, 202(2), 263–274, doi:10.1016/S0012-821X(02)00791-4.
- Montagner, J.-P. (2007), Deep Earth Structure – Upper Mantle Structure: Global Isotropic and Anisotropic Elastic Tomography, *Treatise Geophys.*, 1, 559–589, doi:10.1016/B978-044452748-6.00018-3.
- Montagner, J.-P., and N. Jobert (1988), Vectorial tomography—II. Application to the Indian Ocean, *Geophys. J. Int.*, 94(2), 309–344, doi:10.1111/j.1365-246X.1988.tb05904.x.
- Montagner, J.-P., and H.-C. Nataf (1986), A simple method for inverting the azimuthal anisotropy of surface waves, *J. Geophys. Res.*, 91, 511, doi:10.1029/JB091iB01p00511.
- Montagner, J.-P., and T. Tanimoto (1991), Global upper mantle tomography of seismic velocities and anisotropies, *J. Geophys. Res.*, 96, 20,337, doi:10.1029/91JB01890.
- Mordret, A., D. Rivet, M. Landès, and N. M. Shapiro (2015), Three-dimensional shear velocity anisotropic model of Piton de la Fournaise Volcano (La Réunion Island) from ambient seismic noise, *J. Geophys. Res. Solid Earth*, 120, 406–427, doi:10.1002/2014JB011654.
- Naganjaneyulu, K., and M. Santosh (2012), The nature and thickness of lithosphere beneath the Archean Dharwar Craton, southern India: A magnetotelluric model, *J. Asian Earth Sci.*, 49, 349–361, doi:10.1016/j.jseas.2011.07.002.
- Negi, J. G., O. P. Pandey, and P. K. Agrawal (1986), Super-mobility of hot Indian lithosphere, *Tectonophysics*, 131(1–2), 147–156, doi:10.1016/0040-1951(86)90272-6.
- Nita, B., S. Maurya, and J.-P. Montagner (2016), Anisotropic tomography of the European lithospheric structure from surface wave studies, *Geochem. Geophys. Geosyst.*, 17, 2015–2033, doi:10.1002/2015GC006243.
- O'Neill, C., D. Müller, and B. Steinberger (2003), Geodynamic implications of moving Indian Ocean hotspots, *Earth Planet. Sci. Lett.*, 215(1–2), 151–168, doi:10.1016/S0012-821X(03)00368-6.
- Obrebski, M., R. M. Allen, F. Pollitz, and S.-H. Hung (2011), Lithosphere-asthenosphere interaction beneath the western United States from the joint inversion of body-wave traveltimes and surface-wave phase velocities, *Geophys. J. Int.*, 185(2), 1003–1021, doi:10.1111/j.1365-246X.2011.04990.x.
- Patriat, P., and J. Achache (1984), India–Eurasia collision chronology has implications for crustal shortening and driving mechanism of plates, *Nature*, 311(5987), 615–621, doi:10.1038/311615a0.
- Raval, U., and K. Veeraswamy (2003a), India–Madagascar separation: Breakup along a pre-existing mobile belt and chipping of the craton, *Gondwana Res.*, 6(3), 467–485, doi:10.1016/S1342-937X(05)70999-0.
- Raval, U., and K. Veeraswamy (2003b), Modification of geological and geophysical regimes due to interaction of mantle plume with Indian lithosphere, *J. Virtual Explor.*, 12(12), 117–143, doi:10.3809/jvirtex.2003.00079.
- Rawlinson, N., H. Tkalčić, and A. M. Reading (2010), Structure of the Tasmanian lithosphere from 3D seismic tomography, *Aust. J. Earth Sci.*, 57(4), 381–394, doi:10.1080/08120099.2010.481325.
- Ray, L. (2003), High mantle heat flow in a Precambrian granulite province: Evidence from southern India, *J. Geophys. Res.*, 108(B2), 2084, doi:10.1029/2001JB000688.
- Replumaz, A., A. M. Negrodo, S. Guillot, and A. Villaseñor (2010), Multiple episodes of continental subduction during India/Asia convergence: Insight from seismic tomography and tectonic reconstruction, *Tectonophysics*, 483(1–2), 125–134, doi:10.1016/j.tecto.2009.10.007.
- Replumaz, A., F. A. Capitanio, S. Guillot, A. M. Negrodo, and A. Villaseñor (2014), The coupling of Indian subduction and Asian continental tectonics, *Gondwana Res.*, 26(2), 608–626, doi:10.1016/j.jgr.2014.04.003.
- Ritzwoller, M. H., and A. L. Levshin (1998), Eurasian surface wave tomography: Group velocities, *J. Geophys. Res.*, 103, 4839–4878, doi:10.1029/97JB02622.
- Rodi, W. L., P. Glover, T. M. C. Li, and S. S. Alexander (1975), A fast, accurate method for computing group-velocity partial derivatives for Rayleigh and Love modes, *Bull. Seismol. Soc. Am.*, 65(5), 1105–1114.
- Roy, S., and J.-C. Mareschal (2011), Constraints on the deep thermal structure of the Dharwar Craton, India, from heat flow, shear wave velocities, and mantle xenoliths, *J. Geophys. Res.*, 116, B02409, doi:10.1029/2010JB007796.
- Rychert, C. A., and P. M. Shearer (2009), A global view of the Lithosphere-Asthenosphere boundary, *Science*, 324(5926), 495–498, doi:10.1126/science.1169754.
- Saito, M. (1988), DISPER80: A subroutine package for the calculation of seismic normal-mode solutions, in *Seismological Algorithms—computational methods and computer programs*, edited by D. J. Doornbos, pp. 469, Academic Press, New York.
- Scheingraber, C. (2013), Obspyload: A tool for fully automated retrieval of seismological waveform data, *Seismol. Res. Lett.*, 84(3), 525–531.

- Sebai, A., E. Stutzmann, J. P. Montagner, D. Sicilia, and E. Beucler (2006), Anisotropic structure of the African upper mantle from Rayleigh and Love wave tomography, *Phys. Earth Planet. Inter.*, *155*(1-2), 48–62, doi:10.1016/j.pepi.2005.09.009.
- Selway, K., H. Ford, and P. Kelemen (2015), The seismic mid-lithosphere discontinuity, *Earth Planet. Sci. Lett.*, *414*, 45–57, doi:10.1016/j.epsl.2014.12.029.
- Singh, A., J.-P. Mercier, M. Ravi Kumar, D. Srinagesh, and R. K. Chadha (2014), Continental scale body wave tomography of India: Evidence for attrition and preservation of lithospheric roots, *Geochem. Geophys. Geosyst.*, *15*, 658–675, doi:10.1002/2013GC005056.
- Smith, M. L., and F. A. Dahlen (1973), The azimuthal dependence of Love and Rayleigh wave propagation in a slightly anisotropic medium, *J. Geophys. Res.*, *78*, 3321, doi:10.1029/JB078i017p03321.
- Sodoudi, F., X. Yuan, R. Kind, S. Lebedev, J. M.-C. Adam, E. Kästle, and F. Tilmann (2013), Seismic evidence for stratification in composition and anisotropic fabric within the thick lithosphere of Kalahari Craton, *Geochem. Geophys. Geosyst.*, *14*, 5393–5412, doi:10.1002/2013GC004955.
- Storey, M., and J. Mahoney (1995), Timing of hot spot-related volcanism and the breakup of Madagascar and India, *Science*, *267*, 852–855.
- Takeuchi, H., and M. Saito (1972), Seismic surface waves, in *Methods in Computational Physics*, vol. *11*, pp. 217–295.
- Tarantola, A., and B. Valette (1982), Generalized nonlinear inverse problems solved using the least squares criterion, *Rev. Geophys.*, *20*, 219–232, doi:10.1029/RG020i002p0219.
- Torsvik, T., R. Tucker, L. Ashwal, E. Eide, N. Rakotosolofa, and M. Wit de (1998), Late Cretaceous magmatism in Madagascar: Palaeomagnetic evidence for a stationary Marion hotspot, *Earth Planet. Sci. Lett.*, *164*(1-2), 221–232, doi:10.1016/S0012-821X(98)00206-4.
- Torsvik, T. H., H. Amundsen, E. H. Hartz, F. Corfu, N. Kuszniir, C. Gaina, P. V. Doubrovine, B. Steinberger, L. D. Ashwal, and B. Jamtveit (2013), A Precambrian microcontinent in the Indian Ocean, *Nat. Geosci.*, *6*(3), 223–227, doi:10.1038/ngeo1736.
- Wessel, P., and W. H. F. Smith (1995), New version of the generic mapping tools, *Eos Trans. AGU*, *76*(33), 329, doi:10.1029/95EO00198.
- Wirth, E., and M. D. Long (2010), Frequency-dependent shear wave splitting beneath the Japan and Izu-Bonin subduction zones, *Phys. Earth Planet. Inter.*, *181*(3-4), 141–154, doi:10.1016/j.pepi.2010.05.006.
- Wölbern, I., G. Rümpker, K. Link, and F. Sodoudi (2012), Melt infiltration of the lower lithosphere beneath the Tanzania Craton and the Albertine rift inferred from S receiver functions, *Geochem. Geophys. Geosyst.*, *13*, Q0AK08, doi:10.1029/2012GC004167.
- Yuan, H., and B. Romanowicz (2010), Lithospheric layering in the North American Craton, *Nature*, *466*(7310), 1063–1068, doi:10.1038/nature09332.
- Yuan, H., B. Romanowicz, K. M. Fischer, and D. Abt (2011), 3-D shear wave radially and azimuthally anisotropic velocity model of the North American upper mantle, *Geophys. J. Int.*, *184*(3), 1237–1260, doi:10.1111/j.1365-246X.2010.04901.x.